ARTICLE

Are MXenes Suitable as Cathode Material for Rechargeable Mg Batteries?†

Received 00th January 20xx,
Accepted 00th January 20xx

DOI: 10.1039/x0xx00000x

Henning Kaland,‡[a] Jacob Hadler-Jacobsen,‡[a] Frode Håskjold Fagerli,‡[a] Nils P. Wagner,[ab] Zhaohui Wang,[ac] Sverre M. Selbach,[a] Fride Vullum-Bruer,[ad] Kjell Wiik*[a] and Sondre Kvalvåg Schnell*[a]

MXenes, a type of two-dimensional transition metal carbide/nitride, have received significant interest for electrochemical storage applications. With substantial capacities predicted for Mg-ions, MXenes have been considered a promising candidate for cathode materials for rechargeable Mg batteries (RMBs). While there have been reports demonstrating reversible capacities of 100-200 mA h g^{-1} for MXene-based cathodes, the understanding of the reactions occurring is limited. Here, we investigate unsolvated Mg^{2+}-intercalation into multi-layered, non-delaminated MXene particles by electrochemical characterization of two common MXenes ($Ti_3C_2T_x$ and V_2CT_x) with various electrolytes and at elevated temperatures, complemented by DFT calculations. Our experimental results show poor reversible capacities (< 5 mA h g^{-1}) both at room temperature and at 60 °C, indicating that no intercalation of Mg-ions occurs during cycling. DFT simulations show that $Ti_3C_2T_2$ with fluorine and hydroxyl termination groups has a negative average voltage for Mg^{2+}, and reveal high migration barriers for oxygen termination groups, supporting the experimental results. The DFT calculations also reveal that upon magnesiation in multi-layered V_2CF_2 and $V_2C(OH)_2$, MgF_2 or MgH_2 is formed rather than electrochemical intercalation of Mg^{2+}. However, multi-layered V_2CO_2 is found to have both a relatively high theoretical average voltage (~1.5 V) and a sufficiently low migration barrier of 480 meV, allowing for Mg^{2+} intercalation and RMBs with energy densities comparable to Li-ion batteries. The findings emphasize the need to fully control the MXene termination groups. Possible reasons for the unsatisfactory and deviant electrochemical performance reported in this work and in the literature are critically reviewed to assess the feasibility of MXene cathodes for energy-dense RMBs.

Broader context

Today, lithium-ion batteries (LiBs) represent the state-of-the-art battery technology.Drastic cost reductions and improvements in performance during the last decade, have enabled the ongoing electrification of the transport sector. However, LiBs are facing challenges regarding safety, environmental concerns, high cost and limited availability of raw materials. To meet the future demand for energy storage, new battery technologies addressing these challenges are highly desirable. One of the more prominent candidates is rechargeable magnesium batteries (RMBs), offering a high theoretical energy density and improved safety due to smaller risk of dendrite formation on Mg metal anodes. Nevertheless, the development of RMBs are hindered by the lack of competitive electrolytes and cathode materials, leaving the full potential of RMBs unrealized. One proposed cathode material is MXenes, which already have demonstrated good electrode properties in LiBs. Here, we have evaluated the feasibility of MXene cathodes for energy dense RMBs, by investigating Mg^{2+}-intercalation in two common MXenes. Both the experimental and computational results indicate that the most studied MXene, $Ti_3C_2T_x$, suffers from high migration barriers or unfavourable operating voltages. In contrast, the computational work identified oxygen terminated V_2CO_2 as a more promising candidate and shows the critical importance of controlling the MXene termination groups.

[a] *Department of Materials Science and Engineering, NTNU Norwegian University of Science and Technology, NO-7491 Trondheim, Norway.*
[b] *SINTEF Industry, Sustainable Energy Technology NO-7465 Trondheim, Norway.*
[c] *SINTEF Industry, Metal Production and Processing NO-7465 Trondheim, Norway.*
[d] *SINTEF Energy Research, Thermal Energy, NO-7465 Trondheim, Norway.*
† Electronic Supplementary Information (ESI) available: Full experimental section and additional data are provided. See DOI: 10.1039/x0xx00000x
‡ These authors contributed equally to this work.

1 Introduction

Lithium-ion batteries (LiBs) currently represent the state-of-the-art rechargeable battery technology, but are still limited by factors such as safety and insufficient availability of raw materials.[1] With the expected increase in demand for electric vehicles and grid energy,[2] these limitations may render LiBs inapplicable as the sole solution for rechargeable battery systems. None of the current alternatives are able to compete with the energy density, power density, cycle life and cost of LiBs. However, the theoretical properties and advantage of environmentally friendly compositions of various alternative battery technologies still make them attractive candidates for further investigations.[3, 4] One of these interesting battery technologies is rechargeable magnesium batteries (RMBs), due to the abundance of Mg in the earth's crust, its low cost and the fact that Mg metal is less prone to form dendrites upon cycling than Li metal.[5-7] The latter may enable safe operation of Mg metal anodes, which greatly outperforms today's graphite anode in LiBs in terms of both gravimetric (2205 *vs.* 372 mA h g^{-1}) and volumetric capacity (3833 *vs.* 800 mA h cm^{-3}).[3] Together with the low reduction potential of Mg metal,[8] this opens up for the possibility to have energy-dense batteries based on RMB technology.

Despite the compelling electrode properties of the Mg metal anode, RMBs still face significant challenges in terms of finding compatible electrolytes and suitable cathode materials.[3, 9] Due to the formation of impermeable layers on the Mg anode using common electrolyte salts and solvents, the number of candidates that demonstrate reversible plating/stripping of Mg have generally been limited to ethereal solutions of Mg salts based on Grignard reagents or hydride anions.[10-14] The voltage window of these electrolytes is typically limited to around 2-3 V *vs*. Mg/Mg^{2+}, which therefore leads to the need for high capacity cathode materials in order to have a competitive energy density compared to LiBs.

To date, only a limited number of cathode materials have shown reversible electrochemical reactions with Mg-ions. After the pioneering work of Gregory *et al.*, demonstrating reversible operation in 1990,[15] the first practical RMB prototype is often attributed to the work of Aurbach *et al.* in 2000,[16] who reported excellent cyclability and fast kinetics for their Mo_6S_8 Chevrel phase cathode. Despite its relatively low capacity and operating voltage, it remains one of the best candidates for a secondary battery based on Mg. Since then, various chalcogenides and oxides have been investigated,[17-20] but while the chalcogenides generally suffer from too low operating potentials, the oxides only work at extremely low current densities due to high Mg^{2+} migration barriers.[8] Moreover, cathode materials relying on conversion reactions, particularly sulfur, has gained interest. [21-26] However, detrimental soluble Mg polysulfides inhibit the cycling performance and practical Mg-S batteries.[27] Consequently, there is still an urgent need for Mg cathode materials with sufficient capacity, kinetics and cyclability to enable competitive RMBs.

One interesting group of materials for RMB cathodes is the transition metal carbides, carbonitrides, and nitrides known as MXenes. Since their discovery in 2011,[28] numerous structures have been investigated as electrode materials for various battery chemistries due to its unique two-dimensional structure offering high electronic conductivity, hydrophilicity, tunability and good mechanical strength.[29-33] MXenes have a general composition of $M_{n+1}X_nT_x$ (n = 1,2,3), where M represents an early transition metal (*i.e.* Sc, Ti, V, Cr, Nb, and Mo), X represents carbon and/or nitrogen and T is the surface terminating ion (F, O, and/or OH).[34] Due to their versatile structural possibilities and tuneable surface chemistry, MXenes have been proposed as candidates in a range of applications from sensors to catalysts, as conductive additives and as electrode materials in both supercapacitors and rechargeable batteries.[29, 32, 35] Screening of the intercalation properties of MXenes have shown promising theoretical capacities for Mg-ion intercalation (> 400 mA h g^{-1}),[36, 37] which therefore have attracted interest for RMB research.

The first report on using MXene as cathode material with Mg^{2+} containing ethereal solvents was by Byeon *et al.*[38] With the conventional APC-THF electrolyte, negligible capacities were reported for their freestanding film of delaminated $Ti_3C_2T_x$/carbon nanotube composite cathode. With the addition of 0.4 M LiCl to the electrolyte, significant capacities were observed, assigned solely to Li^+-intercalation by energy-dispersive X-ray spectroscopy (EDX).[38] Recently, several works have reported similar initial capacities for pristine $Ti_3C_2T_x$, all tested with APC-THF electrolyte at room temperature.[39-41] By pre-incorporation of large organic molecules (*e.g.* cationic surfactant,[40] phenyl-MgCl from the electrolyte [41]) or even carbon nanospheres,[39] reversible capacities of 100-200 mA h g^{-1} have been reported. However, all the mentioned works have utilized delaminated $Ti_3C_2T_x$, and combined with the mentioned spacer molecules/structures, a highly porous structure with a large surface area is obtained. The reported voltage profiles differ substantially, and the proposed charge storage mechanisms deviate accordingly; Mg-ion intercalation assisted by cetyltrimethylammonium (CTA^+), phenyl-MgCl intercalation, or a combined intercalation and conversion reaction.[39-41] This raises a critical question about the possibility of unsolvated Mg^{2+} intercalation in MXene, versus predominantly surface reactions and/or intercalation of complex ions. In order to enable competitive energy-dense Mg batteries, intercalation of unsolvated and non-complexed Mg^{2+} ions is necessary. Highly porous structures should therefore be avoided, favouring multi-layered MXene compared to its delaminated counterpart.

In this paper, a systematic investigation on the feasibility of Mg^{2+} intercalation in MXenes for practical rechargeable Mg batteries is presented, combining experiments and Density Functional Theory

(DFT) calculations. First, the MXene structure and morphology is explained, before the proposed charge storage mechanism of MXenes for Mg batteries from literature is critically reviewed. Then, we investigate unsolvated Mg^{2+} intercalation in $Ti_3C_2T_x$, which is the most studied MXene, as well as in $V_2C_2T_x$. The effect of an elevated temperature and electrolytes with different electroactive species are reported. The influence of termination groups (F, O, OH) on Mg^{2+} migration barriers and operating voltages are assessed for both $Ti_3C_2T_x$ and V_2CT_x MXenes. Migration barriers for Li^+ and $MgCl^+$ are also reported to bring further insights to the ion intercalation properties of MXenes and to resolve some of the discrepancies in the reported charge storage mechanisms. The complex relation between the MXene transition metal, the termination groups, single-layer (*i.e.* delaminated) versus multi-layer MXene, and their effect on Mg^{2+} migration barriers and average operating voltages is studied. The findings reveal inherent challenges with some MXene compositions, whereas others stand out as viable cathode candidates. Our work thus provides directions for further efforts to enable MXene cathode materials for rechargeable Mg batteries.

2 Results and discussion

2.1 Structure, intercalation and surface reactions

The peculiar structure of MXenes and different electrolyte-MXene interactions can give rise to different charge storage mechanisms, and may explain some of the deviant electrochemical performance reported for MXene electrodes. Thus, a brief overview on the proposed charge storage mechanism for Li-ions in MXenes is presented, before the reported work on MXenes as RMB cathodes is critically reviewed.

A typical $Ti_3C_2T_x$ MXene particle is illustrated in Figure 1, synthesized by conventional HF etching of the respective Ti_3AlC_2 MAX phase[28, 42] (experimental details in ESI†). The accordion-like morphology is a result of the H_2 evolution during etching,[28] which gives rise to an open structure. Noteworthy, these easily observed large spacings from partly delaminated stacks (ranging from 30-500 nm), referred to as the *interstack* distance, should not be interchanged with the *interlayer* distance between each individual MXene layer (0.9-1.6 nm, shown in inset in Figure 1). True Mg^{2+} intercalation in MXenes should refer to Mg^{2+} insertion between the individual MXene layers, whereas capacity obtained from electrochemical reactions between the stacks will be dominated by adsorption giving pseudocapacitive and/or electrical double-layer charge-storage.

Recently, Okubo *et al.* discussed the deviant voltage profiles reported for MXenes, with an emphasis on Li- and Na-ion intercalation.[43] For aqueous electrolytes, they state that *solvated* cations intercalate between the individual MXene layers, giving a large change in interlayer distance, as well as a change in oxidation state of the metal atom in the MXene. In contrast, in nonaqueous electrolytes, solvated cations may initially intercalate, but the solvation shell quickly collapses and *desolvated* cations continue to intercalate between the MXene layers. Okubo *et al.* named the charge storage mechanism of MXenes in nonaqueous electrolytes after the concept proposed by Augustyn *et al.*; *intercalation pseudocapacitance.*[44] This mechanism is reversible and occurs through ultrafast intercalation of cations with minor structural distortions, little to no diffusion limitations, and a change in the oxidation state of the intercalation host material. A similar charge storage mechanism may be postulated for Mg-ions. However, the reported voltage profiles for non-aqueous Mg-electrolytes deviate and the charge-storage mechanism is far from resolved,[39-41] which will be discussed in the following.

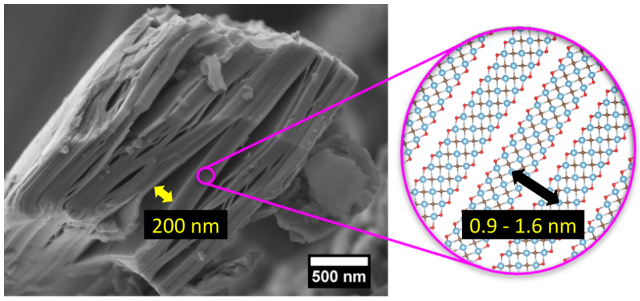

Figure 1. Illustrating the difference between interlayer distance between $Ti_3C_2T_x$ atomic layers (0.9-1.6 nm) and the spacing between stacks of multiple MXene atomic layers (30-500 nm), denoted interstack distance, which is visible in SEM.

Recently, substantial capacities were reported for $Ti_3C_2T_x$ MXene for RMBs, enabled by pre-intercalation of organic molecules or carbon nanospheres.[39, 40] Xu *et al.* reported a cetyltrimethylammonium bromide (CTAB) pre-intercalated $Ti_3C_2T_x$ paper electrode with reversible capacities of ~100 mA h g^{-1} and a sloping voltage profile.[40] Through X-ray photoelectron spectroscopy (XPS) and DFT-simulations, it was proposed that the intercalated surfactant cation, CTA^+, can induce charge transfer from CTA^+ to the MXene. This lowered the Mg diffusion barrier and enabled Mg-ion intercalation, either in the form of unsolvated Mg^{2+} or Mg^{2+} complexed with anions/solvent molecules. *The post mortem* XRD at different states of charge supported a non-trivial reaction mechanism, where the d-spacing of the MXene changed substantially and the original crystallinity was not recovered after charging. Liu *et al.* incorporated CTAB-grafted carbon nanospheres with $Ti_3C_2T_x$ and obtained capacities of around 200 mA h g^{-1} with a similar sloping voltage profile.[39] The increase in MXene d-spacing (0.19 nm) of the $Ti_3C_2T_x$/carbon nanospheres composite was assigned to intercalation of carbon nanospheres, and it was proposed that the expanded interlayers could provide additional diffusion paths and insertion sites for Mg^{2+}-ions. However, it is not clear if the increased d-spacing and improved performance is better explained by intercalation of CTAB, given the similar d-spacing increase (0.20 nm) and observed voltage profile by Xu *et al*.[40] This is further strengthened by the size of the carbon nanospheres, ranging from 100-700 nm in diameter. Still, the carbon nanospheres may seem to preserve the original crystallinity of the $Ti_3C_2T_x$ during cycling, as evidenced by *post*

mortem XRD. The capacity from non-diffusion processes dominated for both reported structures, ranging from 54-82% [40] to 55-92% [39] (depending on scan rate), which indicate predominantly surface-controlled charge storage and limited Mg-ion intercalation. Besides, if the CTA^+ contributes nearly equally as the Mg-ions to the charge storage,[40] the practically obtainable energy density will suffer, as the charge is stored in the electrolyte.

Another noteworthy attempt to enable MXene cathodes for RMBs was recently reported by Zhao *et al.*, demonstrating a 3D macroporous $Ti_3C_2T_x$ paper cathode with clear voltage plateaus and reversible capacities around 200 mA h g^{-1}.[41] The paper cathode was fabricated through a sacrificial template method, obtaining a porosity of around 90%. The highly porous paper was soaked in APC-THF, which lead to increased MXene d-spacing (from 1.36 to 1.55 nm) and substantial amounts of Mg, Al and Cl observed by EDX. This was assigned to pre-intercalation of whole salt molecules from the electrolyte such as $(phenyl\text{-}MgCl)_2AlCl_3$, which subsequently enabled the observed capacities. Through *post mortem* EDX, it was proposed a reversible intercalation/deintercalation of phenyl-MgCl in the first set of discharge/charge plateaus at 2/2.4 V, and a partly irreversible redox reaction between Mg-ions and $Ti_3C_2T_x$ in the second set at 0.8/1.9 V. Thus, a reversible intercalation combined with a partly irreversible conversion mechanism was suggested. Still, it was correctly emphasized the need for more evidence of the redox reactions between Mg-ions and MXenes. For example, the theoretical capacity of $Ti_3C_2T_x$, with equal amount of F, O, OH terminations, is 202 mA h g^{-1}, assuming one Mg per $Ti_3C_2T_x$. At full discharge, a modest Mg content of 0.38 was reported, yet a capacity of ~200 mA h g^{-1} was achieved, indicative of a substantial amount of other electrochemical reactions. Still, the capacity from the first set of discharge/charge plateaus (~45 mA h g^{-1}) matches reasonably well with a one-electron reaction from a 0.38 content of a MgCl compound (40 mA h g^{-1}), justifying the proposed reversible phenyl-MgCl intercalation. For the remaining capacity, a careful *in situ* study may be needed to completely rule out contributions from residual H_2O/proton cycling, or side reactions due to the wide voltage window used.

In summary, the suitability of MXenes as a potential cathode for RMBs is yet to be determined. The above discussion raises a critical question about the feasibility of unsolvated Mg^{2+} intercalation for practical RMBs, which will now be addressed.

2.2 Electrochemical performance and *post mortem* analysis

To assess the suitability of MXenes as intercalation cathodes for Mg batteries, non-delaminated $Ti_3C_2T_x$ powders were tested in coin cells with standard ethereal Mg electrolytes. $Ti_3C_2T_x$ MXene was synthesized by conventional HF etching of the respective Ti_3AlC_2 MAX phase based on previously established methods,[28,42] and is described in detail in the ESI†. Prior to the etching step, ball milling of the Ti_3AlC_2 MAX phase was carried out to ensure a narrow particle size

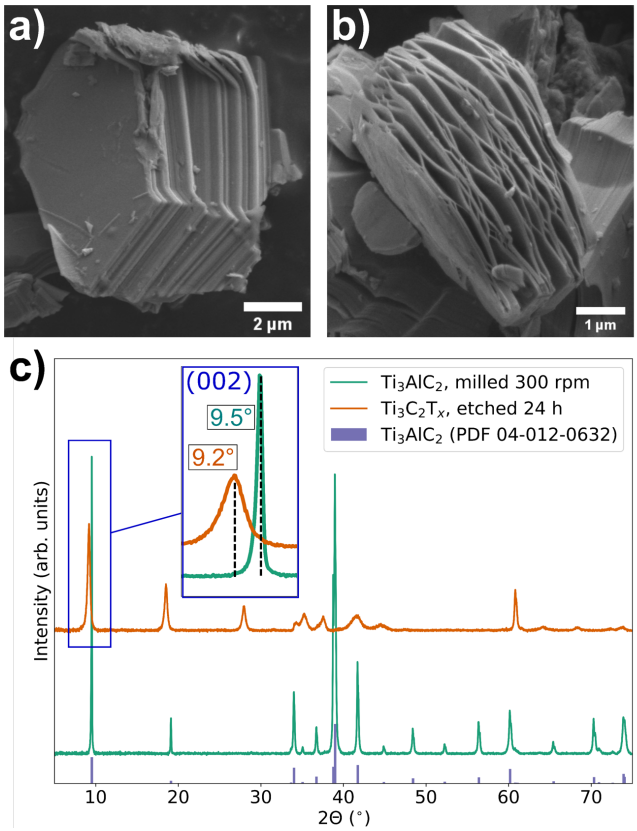

Figure 2. SEM micrographs of (a) Ti_3AlC_2 MAX phase after milling at 300 rpm for 2 h, (b) $Ti_3C_2T_x$ MXene after etching with 10 wt% HF for 24 h showing the accordion-like morphology, and (c) X-ray diffractograms of both compounds confirming the shift of the (002) reflection to larger d-spacing after etching (inset).

distribution of 6 ± 2 µm, as shown in Figure 2a and Figure S1 (ESI†). The milled Ti_3AlC_2 was subsequently etched with 10 wt% HF for 24 h, yielding $Ti_3C_2T_x$ MXene with high phase purity, controlled size distribution and the characteristic accordion-like morphology (Figure 2b). The left-shift of the (002) reflection from $2\Theta_{Ti3AlC2}$ = 9.5° to $2\Theta_{Ti3C2Tx}$ = 9.2° (Figure 2c), corroborated by EDX measurements supporting the absence of aluminium (Table S1), confirmed the complete conversion of MAX phase to MXene. $Ti_3C_2T_x$ cathodes were prepared by wet mixing the MXene powder (80 wt%) with carbon black (10 wt%) and polyvinylidene fluoride (PVDF) (10 wt%) in 1-ethyl-2-pyrrolidone (NEP), before drop casting the slurry on graphite current collector discs. The dried cathodes were electrochemically characterized with a conventional APC-THF electrolyte at a low current density of 10 mA g^{-1} MXene in a voltage window of 0.2 to 2.1 V *vs.* Mg/Mg^{2+}. The resulting voltage profiles are depicted in Figure 3a, demonstrating limited capacities, both at room temperature as well as at an elevated temperature of 60 °C. The initial capacity is slightly higher, approaching 9 mA h g^{-1} at 60 °C, but stabilizes at 3 mA h g^{-1} from the second cycle, with an overall sloped voltage profile. Applying a potentiostatic hold step at 1 mV for 200 h, to allow the sluggish Mg^{2+} diffusion to occur, resulted in increased capacities as seen in Figure 3b. The inset shows how the cathodic current decreases exponentially before stabilizing at ~0.3 µA during the 200 h hold step. However, *post mortem* analysis showed no change in the interlayer distance of $Ti_3C_2T_x$ (Figure 3e), but rather a subtle change

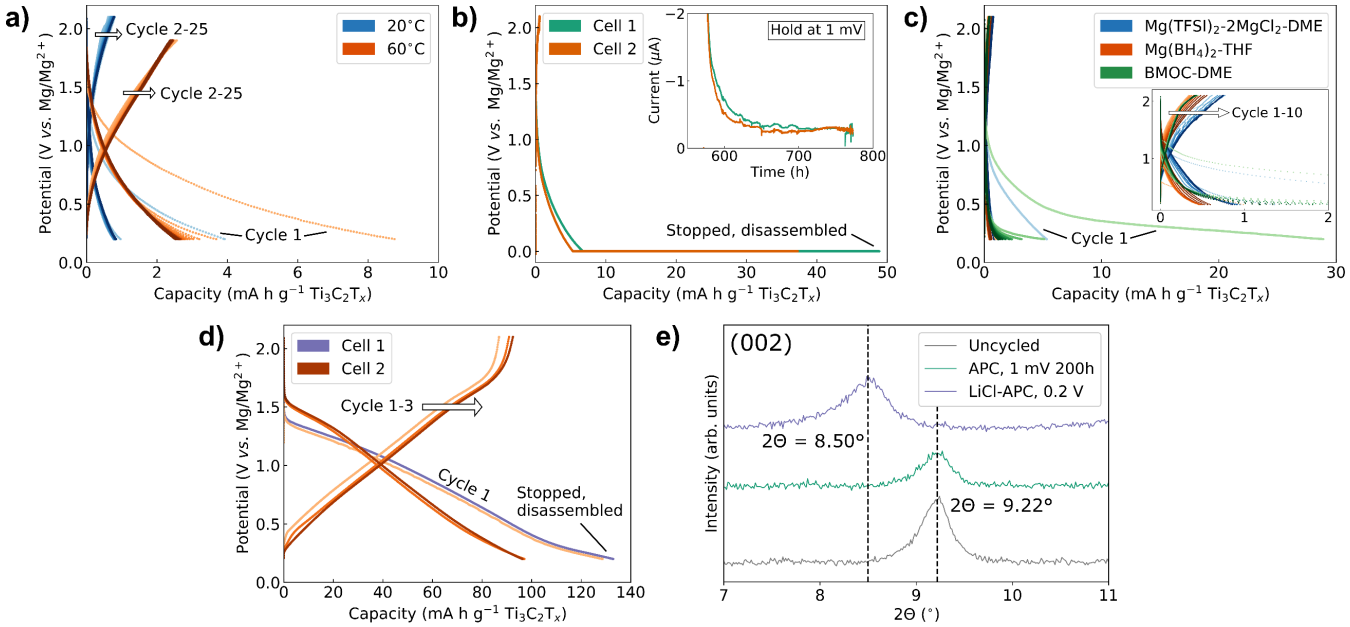

Figure 3. Voltage profiles of $Ti_3C_2T_x$ with APC-THF electrolyte; (a) at 20 °C (blue colour gradient) and 60 °C (orange colour gradient), (b) at 20 °C with a 200 h potentiostatic hold step on 1 mV (inset: cathodic current, thereby negative, as a function of time during the 200 h hold step). (c) Voltage profiles of the ten first cycles of $Ti_3C_2T_x$ with electrolytes of $Mg(TFSI)_2$-$2MgCl_2$-DME (blue colour gradient), $Mg(BH_4)_2$-THF (orange colour gradient) and BMOC-DME (green colour gradient), where inset magnifies the cycling < 2 mA h g^{-1}. (d) APC-THF electrolyte with 0.4 M LiCl (showing two cells, where "Cell 1" was disassembled after 1st discharge). (e) *Post mortem* XRD showing the (002) reflection of $Ti_3C_2T_x$ of an uncycled cell (grey), after the 200 h potentiostatic hold step on 1 mV with APC-THF (cyan, "Cell 1" in (b)), and after being discharged to 0.2 V with APC-THF with 0.4 M LiCl (purple, "Cell 1" in (d)). The colour gradients in (a), (c) and (d) represent increasing cycle number.

in the interlayer Bragg-reflection for graphite (Figure S3) and indication of electrolyte side reactions on the cell bottom casing (Figure S6). Also considering the similar voltage profile and obtained capacities for a carbon black reference electrode (90 wt% carbon black, 10 wt% PVDF on the same graphite paper current collector, shown in Figure S4), Mg^{2+} intercalation in $Ti_3C_2T_x$ MXene is precluded for APC-THF. This is consistent with the majority of earlier work on pristine $Ti_3C_2T_x$ without preintercalation of large molecules cycled in a similar voltage window.[38-40] The discrepancy of the electrochemical performance with the work of Zhao *et al.*[41] is not clear. An initial negligible capacity was reported, but the capacity increased to > 100 mA h g^{-1} even with no preintercalation. It is speculated that the reported highly porous structure (~90% porosity) and large surface area is partly responsible for these capacities, in addition to the already discussed uncertainty in the reaction mechanism.

Given the complex and critical interaction between the cathode and the electrolyte, several other electrolytes were also prepared, verified (Figure S2) and tested (Figure 3c). In the intercalation process, the Mg-ion in the electrolyte must desolvate from the surrounding solvent molecules and/or anions before intercalating into the cathode structure. This critical process may be strongly influenced by the cathode material,[45] and has not been addressed in the reported work on MXene cathodes so far.[38-41] $Mg(TFSI)_2$-$2MgCl_2$-DME contains predominantly the same electroactive cation as APC-THF, namely $MgCl^+$ and/or $Mg_2Cl_3^+$,[11, 46] but solvated by DME instead of THF. As shown by Wang *et al.*, the DME displays substantially lower interaction energies with the $Mg_2Cl_3^+$ dimer compared to THF,[47] which can aid the desolvation process. However, the $Mg(TFSI)_2$-$2MgCl_2$-DME displayed equal electrochemical behaviour as APC-THF (Figure 3c). A thorough evaluation of the Mo_6S_8 Chevrel phase cathode, which is one of the few Mg cathode materials verified to display unsolvated Mg^{2+} intercalation, emphasized the necessity of the cathode material's catalytic ability to break the strong ionic Mg-Cl bond prior to Mg^{2+} intercalation.[45] The Cl-free $Mg(BH_4)_2$-THF electrolyte avoids this issue, having electroactive cations of solvated $[Mg\{(\mu\text{-}H)_2BH_2\}]^+$ and Mg^{2+}.[12] Still, the obtained capacities with this electrolyte were even lower (Figure 3c). Noteworthy, the BMOC-DME electrolyte enabled a relatively high first discharge capacity of nearly 30 mA h g^{-1}, together with a voltage plateau near the cut-off voltage of 0.2 V. The electroactive species of the BMOC-DME electrolyte has been proposed to be $[Mg(DME)_n]^{2+}$ after a conditioning process.[48] This specie circumvents the need of dissociating Mg^{2+} from Cl^-, in addition to benefiting of the presumably lower desolvation energy with DME compared to THF. Lowering the cut-off voltage to 0.01 V *vs.* Mg/Mg^{2+} revealed the appearance of distinct voltage plateaus both on discharge and charge (Figure S5a). Interestingly, *post mortem* XRD proved the intercalation to be in the graphite current collector rather than the MXene (Figure S5b), where the voltage profile and graphite peak change resemble recent reports on co-intercalation of Mg^{2+} with DME/DMF in graphite.[49, 50] In summary, unsolvated Mg^{2+} intercalation in pristine $Ti_3C_2T_x$ MXene was not observed, independent of elevated temperatures and electrolytes.

For comparison, 0.4 M LiCl was added to the APC-THF electrolyte, based on a previous report.[38] With this electrolyte, reversible capacities approaching 100 mA h g^{-1} were obtained (Figure 3d). A

distinct left-shift of the (002) reflection (Figure 3e) is assigned to Li^+ intercalation in $Ti_3C_2T_x$, as also shown by Byeon *et al.*[38] Substantially higher capacities were observed in this work, comparing the performance of pristine $Ti_3C_2T_x$ (~120 mA h g^{-1} *vs.* ~35 mA h g^{-1} at 10 mA g^{-1}). Importantly, as the charge originates from the Li^+ in the electrolyte, the measured capacity is determined by the concentration of LiCl, the amount of electrolyte and the loading of $Ti_3C_2T_x$ per electrode. The electrolyte amount was not reported in the work by Byeon *et al.*, but a similar coin cell (CR2016) and separator (glass fibre) were used, which suggests a similar electrolyte amount. The LiCl concentration was identical, but the $Ti_3C_2T_x$ loading was 2-3 times higher in the work by Byeon *et al.*, offering a likely explanation for the higher capacities reported here. Noteworthy, considering the amount and concentration of LiCl in the electrolyte and the loading of the $Ti_3C_2T_x$ in our work, a capacity of ~560 mA h g^{-1} can be obtained solely by Li-ions, assuming complete utilization of all Li-ions in the electrolyte. This justifies the assignment of the capacity to solely Li-ions. Besides, a carbon black reference electrode (90 wt% carbon black, 10 wt% PVDF on the same graphite paper current collector) demonstrates a significantly different voltage profile and much lower capacities with the same electrolyte (Figure S4), indicating negligible capacity contribution from Li^+ intercalation in the carbon black and/or graphite current collector within the 0.2-2.1 V *vs.* Mg/Mg^{2+} cycling window.

2.3 Migration barriers, average voltages and side reactions

The absence of Mg^{2+} intercalation in $Ti_3C_2T_x$ MXene was further examined by DFT calculations (see ESI† for details). Migration barriers, intercalation energies and average voltages were investigated for both Mg^{2+} and Li^+ in $Ti_3C_2T_2$ and V_2CT_2 with T = F, O and OH surface terminations. Geometrical relaxation was performed, which enabled the identification of side reactions. The utilized unit cells are shown in Figure S9 in the ESI†, where the MXene layers are stacked as mirror images of each other with the Mg layers as the mirror plane (Figure S13). This corresponds to the stacking found experimentally for Na^+ intercalated in $Ti_3C_2T_x$.[51] To bring further understanding of the MXene structure and its electrochemical behaviour, a single-layer of MXene (Figure S9(b, d)) was also studied to mimic adsorption and surface migration on delaminated MXene and on free-standing MXene layers. Both for intercalation in multi-layer and adsorption on single-layer MXene, the most stable site for Mg^{2+} and Li^+ was found to be above a carbon atom, referred to as the C-site (shown in Figure 4a), while the site over the metal (Ti or V, referred to as the M-site) was found to be less favourable (Table S4). The energy barriers for ion migration were calculated for one Mg^{2+}/Li^+ moving from a C-site to a neighbouring metastable M-site using the Climbing Image Nudge Elastic Band (cNEB) method.[52-55] These results were mirrored to give migration energy barrier profiles between two adjacent C-sites. Tests were performed to confirm that the minimum energy path from C-site to the next C-site was via the M-site (see ESI†). Figure 4d shows a typical calculated cNEB profile, with the metastable M-site clearly visible halfway along the migration path. The migration energy barrier profile resembles the shape of Li and Na diffusion in graphite.[56] It is the energy maximum that is reported as the migration barrier. The calculated barriers for single-layer migration on $Ti_3C_2O_2$ MXene are in good agreement with earlier published results.[37, 40] The cNEB profiles for oxygen and fluorine terminated multi-layer $Ti_3C_2T_2$ and $V_2C_2T_2$ with Mg and Li can be found in the ESI† (Figure S10). The DFT results are summarized in Figure 5 and the implications for each MXene composition as a Mg cathode are summarized in Table 1.

Our DFT calculations show that the termination groups strongly dictate the feasibility of MXene cathodes for RMBs. Fluorine and hydroxyl terminations in both multi-layer $Ti_3C_2T_x$ and V_2CT_x give a negative average voltage for Mg^{2+} intercalation and is thus thermodynamically unfavourable (Figure 5b, Table S3). This is in contrast to Li^+ intercalation, which is found to have a positive average voltage for all compositions studied in this work. However, the average voltage is found to be positive for Mg^{2+} into oxygen terminated multi-layer $Ti_3C_2O_2$ and V_2CO_2, having decent values of 1.3 and 1.5 V, respectively. Still, these values assume homogeneous termination groups. Caffrey investigated the effect of mixed surface terminations, where it was found that certain properties, such as the work function, lattice parameters and electronic density of states,

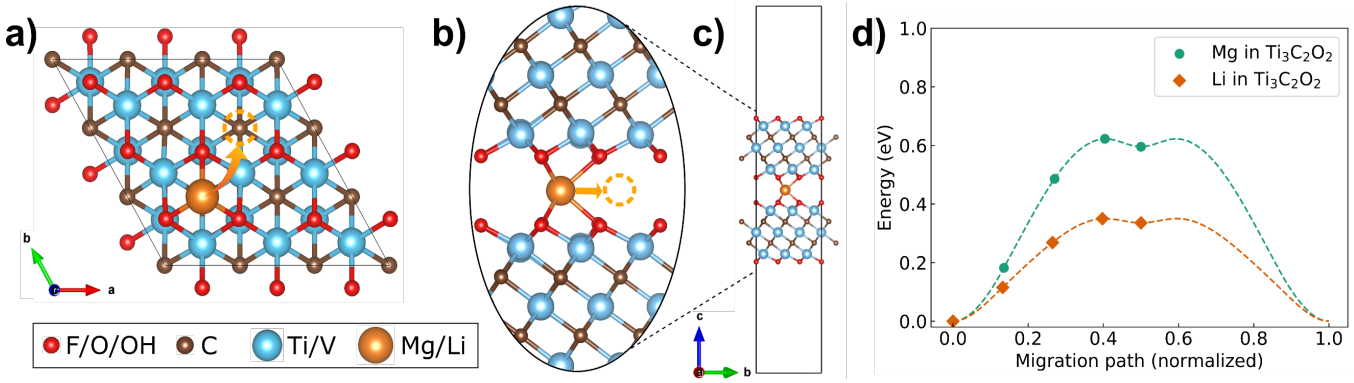

Figure 4. (a) top view of single-layer/multi-layer MXene showing Mg/Li migration from C-site to another C-site via the M-site. (b) side view of the same in multi-layer MXene ($Ti_3C_2O_2$ shown). (c) Unit cell used for simulations on multi-layer MXene ($Ti_3C_2O_2$ shown). (d) Typical calculated cNEB profile of C-site to C-site migration, with the M-site located at the point hallway along the migration path (Mg^{2+} and Li^+ migration in multi-layer $Ti_3C_2O_2$ shown).

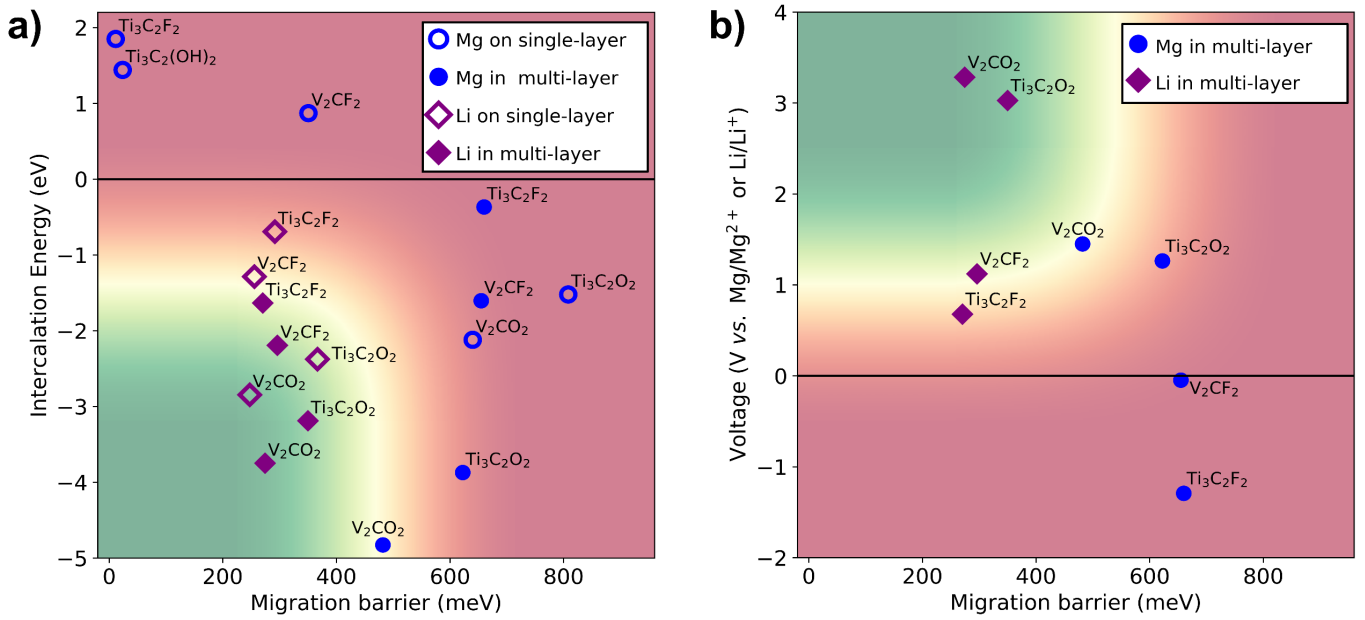

Figure 5. (a) Intercalation energy and migration barriers for fluorine, oxygen and hydroxyl terminated $Ti_3C_2T_2$ and V_2CT_2 MXene by DFT, for both Li^+ (purple diamonds) and Mg^{2+} (blue circles), for single-layer (empty symbols) and multi-layer (filled symbols). (b) Average operation voltages and migration barriers for selected compositions from (a). The green regions represent combinations of sufficiently low migration barriers to allow for useful charging/discharging of 6 µm sized particles at 25 °C,[3] as well as suitable intercalation energies/voltages for practical RMB cathodes. See ESI† for details, and Table S3 for the values presented in these plots.

could be estimated by weighted averages of the results from uniformly terminated MXenes.[57] From Table S1 we see that $Ti_3C_2T_x$ has an O/F ratio of 1.36, while V_2CT_x has an O/F ratio of 0.66. Considering that several recent reports claim that little or no OH terminations will be possible on the Ti_3C_2 surface,[58, 59] we can simplify the estimation by assuming all oxygen content to represent O-terminations. Using a weighted average, we therefore find the adjusted average voltages for the as-synthesized $Ti_3C_2T_x$ and V_2CT_x MXenes to be +0.19 and +0.55 V, respectively. These values indicate spontaneous intercalation of Mg^{2+} in both $Ti_3C_2T_x$ and V_2CT_x, suggesting that the intercalation energy is not a limiting factor for neither of these two structures. Nonetheless, an average voltage of 0.19 or 0.55 V is too low for practical applications, directing further work on oxygen terminated MXenes.

Even though oxygen terminated multi-layer $Ti_3C_2O_2$ showed a decent positive average voltage, Figure 5 also reveals a high migration barrier of 620 meV for Mg^{2+}. According to Canepa *et al.*, a particle size of 6 µm requires a barrier as low as 470 meV at 25 °C or 530 meV at a temperature of 60 °C in order to reach theoretical capacity at a C-rate of C/10 (charging/discharging in 10 h).[3] Thus, for Mg^{2+} in multi-layer $Ti_3C_2O_2$ with a migration barrier of 620 meV, the attainable C-rate becomes approximately 1/3000 at room temperature and 1/500 at 60 °C, in order to be fully charged/discharged. In other words, the high migration barrier of 620 meV appears to strongly limit the performance of $Ti_3C_2O_2$ and may explain the experimental results showing no Mg^{2+} intercalation. However, the relation between migration barriers and attainable C-rates by Canepa *et al.* must be interpreted with great caution. One of the simplifications is that the time needed to fully charge/discharge a spherical particle is approximated the same as the necessary time an ion needs to reach the centre of the particle by random walk. Hence, the model approximates the necessary diffusion length to scale as $\sqrt{Dt}$, where D is the diffusion coefficient and t is the discharge/charge time. Another important assumption is that the model also assumes all kinetic factors other than solid state diffusion to not be rate limiting. Moreover, the presented migration barriers in this work are calculated on a barely discharged MXene cathode (1/9 filling of Mg atoms between two MXene layers in vacuum), and the migration barriers are expected to increase with a higher Mg content.[18] Nonetheless, the model by Canepa *et al.*, combined with DFT, serves as a reasonable indication on which MXenes that may be feasible Mg cathode materials, and which that most likely can be excluded.

Interestingly, the migration barrier for multi-layer V_2CO_2 was calculated to be only 480 meV for Mg^{2+} intercalation, which is below the presumed limit of 530 meV for 6 µm particles. Using the relation between migration barrier and C-rate discussed above, the 480 meV migration barrier for Mg^{2+} corresponds to a C-rate of 1/15 at 25 °C,[3] which should give substantial measurable capacity. To investigate this, V_2CT_x MXene was synthesized and tested as Mg cathodes (see ESI† for details). However, it demonstrated the same poor performance as the $Ti_3C_2T_x$ MXene (Figures S1, S7 and S8). A plausible explanation is a detrimental influence of fluorine and/or hydroxyl terminations. Upon magnesiation, the DFT calculations show that Mg^{2+} reacts with the fluorine and hydroxyl terminations and forms MgF_2 and MgH_2, respectively (Figure S12). Thus, even though the oxygen terminations may enable Mg^{2+} migration, the Mg^{2+} may be trapped irreversibly by the fluorine and/or hydroxyl terminations and block consecutive intercalation. This illustrates the critical need of controlling the termination groups.

Notably, Figure 5a shows that there is no simple correlation between the intercalation energy and the migration energy barrier. The intercalation energy is calculated as the energy difference upon the insertion of one single Mg/Li into the MXene super cell (shown in Figure 4a-c and S9a-d) from a bulk Mg/Li-metal reservoir. Intuitively one could think that a larger energy released upon insertion of Mg/Li would reflect stronger bonds formed and thus also higher migration barriers. This does hold true when comparing *e.g.* Li and Mg in multi-layer V_2CO_2. However, the opposite is seen when comparing V_2CT_2 with $Ti_3C_2T_2$ for the vast majority of the datapoints, *i.e.* V_2CT_2 has both lower migration barriers and higher energy released upon intercalation. As a result, V_2CT_2 appears a much stronger cathode candidate than the most studied $Ti_3C_2T_2$, as it is expected to demonstrate faster diffusion in addition to a higher average voltage.

As expected, Li^+ migration is exceedingly faster than Mg^{2+} for all structures, but the relative difference varies significantly (210-390 meV, Figure S10). Assuming that the ion migration can be approximated proportional to $exp(-E_{migration\ barrier}/k_BT)$ as in transition state theory, every ~60 meV higher migration barrier translates to a factor ten slower migration, at 25 °C. Thus, while Li^+ has a $4.6{\cdot}10^6$ faster diffusion than Mg^{2+} in fluorine terminated $Ti_3C_2F_2$, the difference is reduced to a factor of 3600 in V_2CO_2 (Table S2). The calculated Bader charges provide some insight to this,[60-63] as it assigns the cumulative electronic charge density to atoms, where the atom separation is defined by a minimum in the electronic charge density landscape. It can be seen from Figure S11 that the oxygen is slightly more polarized in $Ti_3C_2O_2$ than in V_2CO_2, which will lead to stronger Mg-O interactions and slower migration. Still, even though excellent rate capability has been reported for Li^+ in MXenes,[64] a 3600 times slower diffusion in V_2CO_2 will inevitably cause a considerably lower power density for Mg^{2+}, or a necessity of operating at an elevated temperature and/or downsizing the particles.

Table 1. Implications of DFT simulations for multi-layered micron sized $Ti_3C_2T_2$ and V_2CT_2 with different termination groups (T = F, O, OH) as Mg cathode materials. The materials need to have a spontaneous intercalation (negative intercalation energy), a migration barrier preferably below 530 meV, and Mg^{2+} intercalation must be more thermodynamically favourable than side reactions (*e.g.* reacting with the termination groups). Only V_2CO_2 passes all criteria.

	Spontaneous intercalation	Migration barrier < 530 meV	Side reactions
$Ti_3C_2F_2$	No	No	No
$Ti_3C_2(OH)_2$	No	N/A	No
$Ti_3C_2O_2$	Yes	No	No
V_2CF_2	No	No	Yes ($^{\alpha}$)
$V_2C(OH)_2$	No	N/A	Yes ($^{\beta}$)
V_2CO_2	Yes	Yes	No

($^{\alpha}$) Formation of MgF_2 is more favourable than Mg^{2+} intercalation.

($^{\beta}$) Formation of MgH_2 is more favourable than Mg^{2+} intercalation.

Noteworthy, the migration barriers decrease considerably when going from single-layer to multi-layer for oxygen terminated $Ti_3C_2O_2$ and V_2CO_2. For instance, the single-layer migration barrier for $Ti_3C_2O_2$ was calculated to be 810 meV and the multi-layer barrier to be 620 meV. Consequently, oxygen terminated multi-layer MXenes look much more promising than their delaminated fluorine-containing counterparts, where V_2CO_2 is the only composition that exhibits spontaneous Mg^{2+} intercalation with a feasible migration barrier and no observed side reactions from DFT calculations.

2.4 Mg^{2+} intercalation in MXenes

Ion intercalation in solids is complex and several critical criteria must be fulfilled. The average voltage must be positive, the ions must be able to enter the structure, and the ions must experience sufficiently low migration barriers in order to have significant intercalation within the particles. The role of the M-element (Ti *vs.* V), the termination groups, single-layer *vs.* multi-layer, and their influence on operating voltages and migration barriers have already been elaborated. High migration barriers and/or detrimental side reactions may explain the observed absence of Mg^{2+} intercalation in $Ti_3C_2T_x$ and V_2CT_x, but that is not the only challenge. The Bader charge analysis may explain the difference between Ti and V based MXene (as discussed earlier), but it also provides direct insight into the complex charge transfer for MXenes. Strikingly, upon magnesiation, the +1.7 charge from Mg is accompanied with a -1.7-charge distributed not only on the transition metal (Ti/V), but also to the oxygen termination group and even the carbon layer (Figure S11). In fact, the ratio of decrease in Bader charge between C : M : O is roughly 1 : 2 : 4, meaning that the largest charge decrease is on the oxygen termination group. This may support a recent X-ray absorption near edge structure (XANES) study that observed only a small change in oxidation state for Ti in parts of the lithiation process of the $Ti_3C_2T_x$ MXene.[65] More importantly, the initial low Bader charge of the transition metal (1.8-2.0 for Ti and 1.8 for V), together with the distributed charge transfer on the transition metal, termination group and carbon layer during discharge, give a reasonable explanation of the calculated low operating voltages. The low voltages constrain the obtainable energy densities, which is addressed in section 2.5.

Another crucial challenge is Mg^{2+} dissociation from the electrolyte, especially in the presence of chlorine ions. As mentioned earlier, the Mg-Cl bond in the $MgCl^+$ species is strong and reported to be over 3000 meV.[66] It has therefore been suggested that the success of the Mo_6S_8 Chevrel phase cathode for Mg batteries is partly due to molybdenum's ability to catalyse the breaking of the $MgCl^+$ bond.[45] Hence, an electrolyte with weakly solvated Mg^{2+} is necessary, or there needs to be some mechanism for Mg^{2+} to desolvate sufficiently easy for intercalation to occur. This last point is critical, as $MgCl^+$ was shown to have a significantly lower migration barrier of 350 meV (Table S3) compared to the 810 meV for Mg^{2+} on single-layer $Ti_3C_2O_2$. Accordingly, if there is space for $MgCl^+$ to intercalate, as in the case

of single-layers or by preintercalation of large molecules, quick migration is to be expected, similar to that of monovalent ions such as Li^+ and Na^+. It has been suggested that the capacity in interlayer expanded TiS_2 cathodes for Mg batteries in fact are due to $MgCl^+$, and not Mg^{2+}.[66] Thus, it would also be important to rule out if the capacity measured with MXene based cathodes in the literature thus far are due to actual Mg^{2+} intercalation, or the much less desirable $MgCl^+$ intercalation. This is especially relevant for MXenes, where spacer molecules can be used to increase the interlayer distance such as in Refs. [33, 66] As discussed earlier, Zhao *et al.* assigned the first set of discharge/charge voltage plateaus for their $Ti_3C_2T_x$ cathode to be reversible phenyl-MgCl intercalation. The low migration barrier reported for $MgCl^+$ here, may support the proposed mechanism, or at least support the intercalation of a monovalent $MgCl^+$ compound. The reason $MgCl^+$-intercalation is undesirable is that only the Mg constituent is stored densely in the Mg metal anode, while an excessive amount of electrolyte is needed to store the corresponding amount of chloride ions. The weight and volume added by the excessive amount of electrolyte will limit the energy density. This also highlights the need for reporting the amount of electrolyte, in addition to cathode loading.

Even if the Mg^{2+} desolvation and anion dissociation is successful and the migration barriers inside the MXene are low, Mg^{2+} intercalation also depends on the local environment at the MXene edges. It is well established that the MXene surface is negatively charged, but a recent study also found the edges to be positively charged.[67] This will unavoidably lead to electrostatic repulsion between the MXene edge and the incoming Mg-ions, and further complicates the cathode-electrolyte interface and desolvation process. Considering the stability of MgO, MgF_2, $Mg(OH)_2$ and MgH_2 as possible by-products, it is also likely that initial Mg^{2+} reacts irreversibly with the termination groups at the particle edge and blocks further Mg^{2+} intercalation. This was found to happen spontaneously with V_2CF_2 and $V_2C(OH)_2$ in our DFT calculations (Figure S12), indicating that MgV_2CF_2 and $MgV_2C(OH)_2$ are very unstable.

2.5 MXenes as a rechargeable Mg battery cathode material

The MXene group of materials shows complex and flexible chemistries resulting in a large number of possible cathode designs, and this section aims to evaluate the potential of MXenes as RMB cathodes. Our DFT calculations show that both the elemental composition and the termination groups are imperative. Somewhat unexpected and in contrast to the experimental approach reported in the literature, multi-layer MXene seems more promising than its single-layer counterpart, both in terms of lower migration barriers, higher average voltages and its denser structure. Preintercalation of spacers does not appear a good approach, where the increased interlayer distance may give a single-layer type behaviour and solvated Mg-ion complexes may intercalate instead of Mg^{2+}. The relatively high average voltage and low migration barriers for oxygen terminated V_2CO_2 MXene suggests that Mg^{2+} intercalation may be possible. However, as fluorine and hydroxyl terminations give rise to unwanted side-reactions, and since no reversible intercalation was observed experimentally for V_2CT_x with mixed terminations, controlling the termination group seems to be of critical importance.

Uniformly oxygen terminated V_2CO_2 stands out as a possible RMB cathode candidate. Given its calculated average voltage of 1.5 V and theoretical capacity of 367 mA h g^{-1} (based on 1 layer of Mg^{2+} intercalation, MgV_2CO_2, and 2 electrons per Mg-ion), this gives a material specific energy of 551 W h kg^{-1}. This is comparable to the specific energy of $LiMn_2O_4$ (*vs.* a graphite anode with a redox potential of 0.2 V *vs.* Li/Li^+) for Li-ion batteries.[68] V_2CO_2 has a relatively high material density of 4.79 g cm^{-3}, yielding an impressive volumetric energy density of 2640 W h l^{-1} at the material level. However, this value is for dense multi-layered particles without the mentioned interstack distance. Still, if we consider a lower and more practically obtainable density of 1.5 g cm^{-3}, this will be compensated by the high volumetric capacity of the Mg anode. As a result, a full cell with a V_2CO_2 cathode and a Mg anode (with 0% Mg excess) has a high theoretical specific energy of 472 W h kg^{-1} and may reach a volumetric energy density of 723 W h l^{-1}, only considering the active materials and a V_2CO_2 density of 1.5 g cm^{-3}. In comparison, a $LiFePO_4$ – graphite full cell (1:1 capacity balanced) has a practical specific energy of 324 W h kg^{-1} and volumetric energy density of 724 W h l^{-1}, also considering the active materials only and a $LiFePO_4$ packing density of 2 g cm^{-3}.[69]

Nevertheless, the viable energy densities of V_2CO_2 depends on uniformly terminated V_2CO_2, which pose a crucial challenge. Recent work on fluorine-free synthesis of $Ti_3C_2T_x$ gives some promise,[70-74] but a similar synthesis approach may not be feasible for V_2CO_2 given the much harsher etching conditions required for V_2CT_x, indicative of substantially stronger metal-aluminium bonds.[75] Furthermore, the prerequisite of having Mg^{2+} successfully desolvating from the electrolyte and entering the interlayers still remains. These issues demand a critical assessment of the electrolyte-cathode interface and better fundamental understanding of the MXene surface chemistry, as well as our ability to fully control them. The above discussion leaves MXenes, with the right composition and structure, as a theoretically viable Mg cathode candidate, but with significant challenges for experimental realization. Further thorough screening of the around 20 other MXenes[29] may also reveal other candidates for practical cathode materials for RMBs. Finally, the findings and critical aspects discussed herein are not only applicable to RMBs, and we believe the new insights can accelerate the research for MXene-based electrodes for other chemistries as well, such as Li-, Na-, K-, Ca- and Al-ion batteries.

3 Conclusions

In summary, we have assessed the promise and reality of MXenes as a potential cathode material for practical RMBs, combining experiments and atomistic computer simulations. Multi-layered $Ti_3C_2T_x$ and V_2CT_x MXenes were not observed to intercalate

unsolvated Mg^{2+} at an elevated temperature of 60 °C, and regardless of electrolytes. The DFT calculations showed that the intercalation energies and migration barriers heavily depend on both the elemental composition and the termination groups of the MXenes. The most studied MXene, $Ti_3C_2T_x$, is precluded as a feasible Mg cathode candidate, where hydroxyl and fluorine terminations resulted in thermodynamically unfavourable average voltages and oxygen termination resulted in high migration barriers. However, oxygen terminated V_2CO_2 MXene is identified as a viable cathode candidate, as it shows a combination of decent average operating potential (1.5 V) and feasible Mg^{2+} migration barriers. Still, side reactions of Mg^{2+} with the fluorine and/or hydroxyl terminations resulting in MgF_2/MgH_2, seems detrimental to Mg^{2+} intercalation in as-synthesized V_2CT_x, in addition to the challenges related to the non-trivial desolvation of Mg^{2+} from the electrolyte. The current results indicate that the MXene 'M'-elements, termination groups and degree of delamination must all be carefully assessed to allow unsolvated Mg^{2+} intercalation. More research on the above-mentioned challenges, especially controlling the termination groups, is required to realize the theoretical potential of MXenes for energy dense RMB cathodes.

Supplementary information

A full description of the experimental and computational methods used in this work is given in the Supplementary information (ESI†). Additional figures and tables are also included there.

Conflicts of interest

There are no conflicts to declare.

Acknowledgements

This work was financially supported by the Research Council of Norway through a FRINATEK project, project number 275810, and through the Department of Materials Science and Engineering at NTNU Norwegian University of Science and Technology. We would also like to acknowledge Lars-Arne Boge for performing the synthesis of the V_2CT_x MXene and preparing the V_2CT_x-cathodes, and Tor Grande for valuable discussions. Sigma2 is acknowledged for CPU-time through project number NN9414K and NN9264K.

Notes and references

1. Y. Ding, Z. P. Cano, A. Yu, J. Lu and Z. Chen, *Electrochemical Energy Reviews*, 2019, **2**, 1-28.
2. G. Zubi, R. Dufo-López, M. Carvalho and G. Pasaoglu, *Renewable and Sustainable Energy Reviews*, 2018, **89**, 292-308.
3. P. Canepa, G. Sai Gautam, D. C. Hannah, R. Malik, M. Liu, K. G. Gallagher, K. A. Persson and G. Ceder, *Chemical Reviews*, 2017, **117**, 4287-4341.
4. J. W. Choi and D. Aurbach, *Nature Reviews Materials*, 2016, **1**, 16013.
5. C. Ling, D. Banerjee and M. Matsui, *Electrochimica Acta*, 2012, **76**, 270-274.
6. M. Matsui, *Journal of Power Sources*, 2011, **196**, 7048-7055.
7. P. C. K. Vesborg and T. F. Jaramillo, *RSC Advances*, 2012, **2**, 7933-7947.
8. M. Mao, T. Gao, S. Hou and C. Wang, *Chemical Society Reviews*, 2018, **47**, 8804-8841.
9. R. Mohtadi and F. Mizuno, *Beilstein Journal of Nanotechnology*, 2014, **5**, 1291-1311.
10. N. Amir, Y. Vestfrid, O. Chusid, Y. Gofer and D. Aurbach, *Journal of Power Sources*, 2007, **174**, 1234-1240.
11. P. Canepa, S. Jayaraman, L. Cheng, N. N. Rajput, W. D. Richards, G. S. Gautam, L. A. Curtiss, K. A. Persson and G. Ceder, *Energy & Environmental Science*, 2015, **8**, 3718-3730.
12. R. Mohtadi, M. Matsui, T. S. Arthur and S.-J. Hwang, *Angewandte Chemie International Edition*, 2012, **51**, 9780-9783.
13. I. Shterenberg, M. Salama, Y. Gofer and D. Aurbach, *Langmuir*, 2017, **33**, 9472-9478.
14. H. D. Yoo, I. Shterenberg, Y. Gofer, G. Gershinsky, N. Pour and D. Aurbach, *Energy & Environmental Science*, 2013, **6**, 2265-2279.
15. T. D. Gregory, R. J. Hoffman and R. C. Winterton, *Journal of The Electrochemical Society*, 1990, **137**, 775-780.
16. D. Aurbach, Z. Lu, A. Schechter, Y. Gofer, H. Gizbar, R. Turgeman, Y. Cohen, M. Moshkovich and E. Levi, *Nature*, 2000, **407**, 724-727.
17. G. Gershinsky, H. D. Yoo, Y. Gofer and D. Aurbach, *Langmuir*, 2013, **29**, 10964-10972.
18. X. Sun, P. Bonnick, V. Duffort, M. Liu, Z. Rong, K. A. Persson, G. Ceder and L. F. Nazar, *Energy & Environmental Science*, 2016, **9**, 2273-2277.
19. X. Sun, P. Bonnick and L. F. Nazar, *ACS Energy Letters*, 2016, **1**, 297-301.
20. L. Wang, K. Asheim, P. E. Vullum, A. M. Svensson and F. Vullum-Bruer, *Chemistry of Materials*, 2016, **28**, 6459-6470.
21. A. Du, Z. Zhang, H. Qu, Z. Cui, L. Qiao, L. Wang, J. Chai, T. Lu, S. Dong, T. Dong, H. Xu, X. Zhou and G. Cui, *Energy & Environmental Science*, 2017, **10**, 2616-2625.
22. H. O. Ford, L. C. Merrill, P. He, S. P. Upadhyay and J. L. Schaefer, *Macromolecules*, 2018, **51**, 8629-8636.
23. T. Gao, S. Hou, F. Wang, Z. Ma, X. Li, K. Xu and C. Wang, *Angewandte Chemie International Edition*, 2017, **56**, 13526-13530.
24. H. S. Kim, T. S. Arthur, G. D. Allred, J. Zajicek, J. G. Newman, A. E. Rodnyansky, A. G. Oliver, W. C. Boggess and J. Muldoon, *Nature Communications*, 2011, **2**, 427.
25. Z. Zhao-Karger, M. E. Gil Bardaji, O. Fuhr and M. Fichtner, *Journal of Materials Chemistry A*, 2017, **5**, 10815-10820.
26. Z. Zhao-Karger, X. Zhao, D. Wang, T. Diemant, R. J. Behm and M. Fichtner, *Advanced Energy Materials*, 2015, **5**, 1401155.
27. M. Salama, R. Attias, B. Hirsch, R. Yemini, Y. Gofer, M. Noked and D. Aurbach, *ACS Applied Materials & Interfaces*, 2018, **10**, 36910-36917.

28. M. Naguib, M. Kurtoglu, V. Presser, J. Lu, J. Niu, M. Heon, L. Hultman, Y. Gogotsi and M. W. Barsoum, *Advanced Materials*, 2011, **23**, 4248-4253.
29. B. Anasori, M. R. Lukatskaya and Y. Gogotsi, *Nature Reviews Materials*, 2017, **2**, 16098.
30. D. Er, J. Li, M. Naguib, Y. Gogotsi and V. B. Shenoy, *ACS Applied Materials & Interfaces*, 2014, **6**, 11173-11179.
31. F. Ming, H. Liang, W. Zhang, J. Ming, Y. Lei, A.-H. Emwas and H. N. Alshareef, *Nano Energy*, 2019, **62**, 853-860.
32. M. Naguib, J. Halim, J. Lu, K. M. Cook, L. Hultman, Y. Gogotsi and M. W. Barsoum, *Journal of the American Chemical Society*, 2013, **135**, 15966-15969.
33. A. VahidMohammadi, A. Hadjikhani, S. Shahbazmohamadi and M. Beidaghi, *ACS Nano*, 2017, **11**, 11135-11144.
34. M. Naguib, V. N. Mochalin, M. W. Barsoum and Y. Gogotsi, *Advanced Materials*, 2014, **26**, 992-1005.
35. M. R. Lukatskaya, S. Kota, Z. Lin, M.-Q. Zhao, N. Shpigel, M. D. Levi, J. Halim, P.-L. Taberna, M. W. Barsoum, P. Simon and Y. Gogotsi, *Nature Energy*, 2017, **2**, 17105.
36. C. Eames and M. S. Islam, *Journal of the American Chemical Society*, 2014, **136**, 16270-16276.
37. Y. Xie, Y. Dall'Agnese, M. Naguib, Y. Gogotsi, M. W. Barsoum, H. L. Zhuang and P. R. C. Kent, *ACS Nano*, 2014, **8**, 9606-9615.
38. A. Byeon, M.-Q. Zhao, C. E. Ren, J. Halim, S. Kota, P. Urbankowski, B. Anasori, M. W. Barsoum and Y. Gogotsi, *ACS Applied Materials & Interfaces*, 2017, **9**, 4296-4300.
39. F. Liu, Y. Liu, X. Zhao, X. Liu and L.-Z. Fan, *Journal of Materials Chemistry A*, 2019, **7**, 16712-16719.
40. M. Xu, S. Lei, J. Qi, Q. Dou, L. Liu, Y. Lu, Q. Huang, S. Shi and X. Yan, *ACS Nano*, 2018, **12**, 3733-3740.
41. M.-Q. Zhao, C. E. Ren, M. Alhabeb, B. Anasori, M. W. Barsoum and Y. Gogotsi, *ACS Applied Energy Materials*, 2019, **2**, 1572-1578.
42. M. Alhabeb, K. Maleski, B. Anasori, P. Lelyukh, L. Clark, S. Sin and Y. Gogotsi, *Chemistry of Materials*, 2017, **29**, 7633-7644.
43. M. Okubo, A. Sugahara, S. Kajiyama and A. Yamada, *Accounts of Chemical Research*, 2018, **51**, 591-599.
44. V. Augustyn, J. Come, M. A. Lowe, J. W. Kim, P.-L. Taberna, S. H. Tolbert, H. D. Abruña, P. Simon and B. Dunn, *Nature Materials*, 2013, **12**, 518.
45. L. F. Wan, B. R. Perdue, C. A. Apblett and D. Prendergast, *Chemistry of Materials*, 2015, **27**, 5932-5940.
46. N. Pour, Y. Gofer, D. T. Major and D. Aurbach, *Journal of the American Chemical Society*, 2011, **133**, 6270-6278.
47. L. Wang, B. Jiang, P. E. Vullum, A. M. Svensson, A. Erbe, S. M. Selbach, H. Xu and F. Vullum-Bruer, *ACS Nano*, 2018, **12**, 2998-3009.
48. H. Xu, Z. Zhang, Z. Cui, A. Du, C. Lu, S. Dong, J. Ma, X. Zhou and G. Cui, *Electrochemistry Communications*, 2017, **83**, 72-76.
49. C. God, B. Bitschnau, K. Kapper, C. Lenardt, M. Schmuck, F. Mautner and S. Koller, *RSC Advances*, 2017, **7**, 14168-14175.
50. D.-M. Kim, S. C. Jung, S. Ha, Y. Kim, Y. Park, J. H. Ryu, Y.-K. Han and K. T. Lee, *Chemistry of Materials*, 2018, **30**, 3199-3203.
51. X. Wang, X. Shen, Y. Gao, Z. Wang, R. Yu and L. Chen, *Journal of the American Chemical Society*, 2015, **137**, 2715-2721.
52. G. Henkelman, G. Jóhannesson and H. Jónsson, in *Theoretical Methods in Condensed Phase Chemistry*, ed. S. D. Schwartz, Springer Netherlands, Dordrecht, 2002, DOI: 10.1007/0-306-46949-9_10, pp. 269-302.
53. G. Henkelman and H. Jónsson, *The Journal of Chemical Physics*, 2000, **113**, 9978-9985.
54. G. Henkelman, B. P. Uberuaga and H. Jónsson, *The Journal of Chemical Physics*, 2000, **113**, 9901-9904.
55. D. Sheppard, R. Terrell and G. Henkelman, *The Journal of Chemical Physics*, 2008, **128**, 134106.
56. Z. Wang, A. P. Ratvik, T. Grande and S. M. Selbach, *RSC Advances*, 2015, **5**, 15985-15992.
57. N. M. Caffrey, *Nanoscale*, 2018, **10**, 13520-13530.
58. M. A. Hope, A. C. Forse, K. J. Griffith, M. R. Lukatskaya, M. Ghidiu, Y. Gogotsi and C. P. Grey, *Physical Chemistry Chemical Physics*, 2016, **18**, 5099-5102.
59. I. Persson, L.-Å. Näslund, J. Halim, M. W. Barsoum, V. Darakchieva, J. Palisaitis, J. Rosen and P. O. Å. Persson, *2D Materials*, 2017, **5**, 015002.
60. G. Henkelman, A. Arnaldsson and H. Jónsson, *Computational Materials Science*, 2006, **36**, 354-360.
61. E. Sanville, S. D. Kenny, R. Smith and G. Henkelman, *Journal of Computational Chemistry*, 2007, **28**, 899-908.
62. W. Tang, E. Sanville and G. Henkelman, *Journal of Physics: Condensed Matter*, 2009, **21**, 084204.
63. M. Yu and D. R. Trinkle, *The Journal of Chemical Physics*, 2011, **134**, 064111.
64. D. Sun, M. Wang, Z. Li, G. Fan, L.-Z. Fan and A. Zhou, *Electrochemistry Communications*, 2014, **47**, 80-83.
65. Y. Xie, M. Naguib, V. N. Mochalin, M. W. Barsoum, Y. Gogotsi, X. Yu, K.-W. Nam, X.-Q. Yang, A. I. Kolesnikov and P. R. C. Kent, *Journal of the American Chemical Society*, 2014, **136**, 6385-6394.
66. H. D. Yoo, Y. Liang, H. Dong, J. Lin, H. Wang, Y. Liu, L. Ma, T. Wu, Y. Li, Q. Ru, Y. Jing, Q. An, W. Zhou, J. Guo, J. Lu, S. T. Pantelides, X. Qian and Y. Yao, *Nature Communications*, 2017, **8**, 339.
67. V. Natu, M. Sokol, L. Verger and M. W. Barsoum, *The Journal of Physical Chemistry C*, 2018, **122**, 27745-27753.
68. R. Schmuch, R. Wagner, G. Hörpel, T. Placke and M. Winter, *Nature Energy*, 2018, **3**, 267-278.
69. P. Meister, H. Jia, J. Li, R. Kloepsch, M. Winter and T. Placke, *Chemistry of Materials*, 2016, **28**, 7203-7217.
70. M. Li, J. Lu, K. Luo, Y. Li, K. Chang, K. Chen, J. Zhou, J. Rosen, L. Hultman, P. Eklund, P. O. Å. Persson, S. Du, Z. Chai, Z. Huang and Q. Huang, *Journal of the American Chemical Society*, 2019, **141**, 4730-4737.
71. T. Li, L. Yao, Q. Liu, J. Gu, R. Luo, J. Li, X. Yan, W. Wang, P. Liu, B. Chen, W. Zhang, W. Abbas, R. Naz and D. Zhang, *Angewandte Chemie International Edition*, 2018, **57**, 6115-6119.
72. J. Lu, I. Persson, H. Lind, J. Palisaitis, M. Li, Y. Li, K. Chen, J. Zhou, S. Du, Z. Chai, Z. Huang, L. Hultman, P. Eklund, J. Rosen, Q. Huang and P. O. Å. Persson, *Nanoscale Advances*, 2019, **1**, 3680-3685.
73. S. Yang, P. Zhang, F. Wang, A. G. Ricciardulli, M. R. Lohe, P. W. M. Blom and X. Feng, *Angewandte Chemie International Edition*, 2018, **57**, 15491-15495.
74. B. Zhang, J. Zhu, P. Shi, W. Wu and F. Wang, *Ceramics International*, 2019, **45**, 8395-8405.

75. V. M. Hong Ng, H. Huang, K. Zhou, P. S. Lee, W. Que, J. Z. Xu and L. B. Kong, *Journal of Materials Chemistry A*, 2017, **5**, 3039-3068.

